Phased chromosome-scale genome assembly of an asexual, allopolyploid root-knot nematode reveals complex subgenomic structure

Analysis of the allopolyploid genome of *Meloidogyne javanica*

Michael R Winter[1*], Adam P Taranto[3], Henok Zemene Yimer[2], Alison Coomer-Blundell[3], Shahid Siddique[2], Valerie M Williamson[3], and David H Lunt[1]

[1]School of Natural Sciences, University of Hull, Hull, UK

[2]Department of Entomology and Nematology, University of California Davis, Davis CA, USA

[3]Department of Plant Pathology, University of California Davis, Davis CA, USA

*Corresponding author

E-mail: mrmrwinter@gmail.com (MRW)

Abstract

We present the chromosome-scale genome of the allopolyploid root-knot nematode *Meloidogyne javanica*. We show that the *M. javanica* genome is predominantly allotetraploid, comprising two subgenomes, A and B, that most likely originated from hybridisation of two ancestral parental species. The assembly is annotated using full-length non-chimeric transcripts, comparison to reference databases, and *ab initio* prediction techniques, and the subgenomes are phased using ancestral k-mer spectral analysis. Subgenome B appears to show greater fission of chromosomal contigs, and while there is substantial synteny between subgenomes, we also identify regions lacking synteny that may have diverged in the ancestral genomes prior to or following hybridisation. Indels are common both between alleles within a subgenome, and between the A and B subgenomes, suggesting the *M. javanica* genome exists in a dynamic hypo-tetraploidy where copy number can vary along the chromosome. This annotated and phased genome assembly forms a significant resource for understanding the origins and genetics of these globally important plant pathogens.

Author Summary

Root-knot nematodes represent one of the most significant crop parasites globally. Despite their agricultural importance, only rudimentary genomic resources have been published to date, leaving a gap in the understanding of genetic mechanisms driving genome evolution and crop virulence. Here, we have used modern genomic and bioinformatic approaches to create a chromosome-scale reference genome to investigate the origins and genomic constitution of the root-knot nematode species *Meloidogyne javanica*. This species reproduces by ameiotic parthenogenesis and has an allopolyploid

genome and is among the most damaging plant parasitic nematodes with a large and evolving plant host range.

Utilising modern long-range DNA sequencing and bioinformatics approaches, we successfully phased the genome into its constituent subgenomes, a first for this agriculturally important clade. While we find the genomic landscape is mostly syntenic between subgenomes, we identified regions of minimal similarity, and highlight structural divergence between subgenomes. We demonstrate that this species was originally tetraploid, but insertions and deletions have been the major force in generating diversity, resulting in a hypo-tetraploid genome with local variations in ploidy.

Introduction

The assembly of allopolyploid genomes

Allopolyploidy is a genomic state characterised by more than two chromosomal complements, with one or more of these complements resulting from a hybridisation event leading to the presence of distinct (homoeologous) subgenomes within a single cell [1]. Allopolyploids may account for 11% of plant species including many model species and important crops [2]. Although not as frequent as in plants, genomic investigations are indicating that ancestral genome duplication, hybridisation, and complex genome arrangements are more widespread than previously recognized in animals [3,4]. Assembly and analysis of allopolyploid genomes, however, is challenging for a number of reasons [5]. The increased number of alleles within an allopolyploid genome can interfere with algorithms used by many assemblers leading to the accumulation of switch errors; regions of the assembly where the sequence switches between haplotypes or homoeologs. In addition, the high amount of repeat content often found in allopolyploid genomes can result

in fragmentation of the final assembly if sequenced reads fail to span the repeat [6,7]. Another difficulty in accurate assembly of allopolyploid genomes has been 'phasing' ie, the assignment of assembly contigs to the correct subgenome. Switch errors and misassemblies introduced during the assembly process can impair the signals required to successfully phase a scaffold, and potential crossover interactions between homoeologs can further complicate this signal [8,9].

Assembly of allopolyploid genomes has become more feasible due to the advent of long-read sequencing technologies and better assembly algorithms. Most chromosome-scale allopolyploid assemblies in the literature are of agricultural plants [10–13], although a few chromosome-scale allopolyploid assemblies of animal genomes are now also available [14,15].

Root-knot nematodes

Root-knot nematodes (RKN) - genus Meloidogyne - are a group of obligate plant parasites that include species which severely reduce crop yield [16]. Second-stage juveniles (J2s) of RKNs hatch in the soil and are non-feeding, needing to invade a host plant root to complete their life cycle. Upon reaching the vascular cylinder, J2s induce the formation of a feeding site inside the root, characterised by formation of a gall ("root-knot") and highly modified "giant cells" on which the nematode feeds [17]. Three closely related species within the Meloidogyne genus, M. arenaria, M. incognita, and M. javanica, which we refer to here as the Meloidogyne incognita group (MIG), have extremely broad host ranges spanning the majority of flowering plants [18,19]) and together are estimated to cost the agricultural industry tens of billions of US dollars a year [20–22]. Almost 100 RKN species have been described [23,24], which differ in host range, pathogenicity, geographic range, morphology and reproductive mode.

Although RKN nematodes species have diverse modes of reproduction including amphimixis, automixis, and obligate apomixis, cytological examination indicates that M. javanica and most other MIG species reproduce by mitotic parthenogenesis; that is, maturation of oocytes consists of a single mitotic division in which chromosomes remain univalent at metaphase [25,26]. Phylogenomic analysis has revealed that each species possesses two divergent copies of many genes, that the three species likely originated from interspecific hybridisation, and that they share the same ancestors who have provided the A and B subgenomes [19,27,28].

Despite asexual reproduction, field isolates and greenhouse selections of MIG species are diverse and successful, differing in their ability to reproduce on specific crop species and varieties (Hartman and Sasser, 1985; [20,29–31]. A widely investigated example is acquisition of ability to reproduce on tomato with the resistance gene Mi-1, which confers effective resistance to MIG species and is widely deployed for nematode management in tomato [32]. Many independent studies have identified MIG populations that are able to break Mi-mediated resistance; these include both field isolates and greenhouse selections of isofemale lines [33,34]. However, efforts to decipher the genetic mechanisms for these phenotypic variants have not so far been successful due in part to the lack of tractable genetics and limitations in genome assemblies. Current MIG genome assemblies are fragmented and the homoeologous genomes are mostly unphased [19,28,35,36] making it difficult to compare homoeologous sequences, gain a true picture of diversity, or to understand the nature of functional variation.

Here we apply a combination of modern genomic and bioinformatic approaches to generate a highly-contiguous, chromosome-level assembly of M. javanica, phased into two subgenomes, creating the first chromosome-scale genome assembly of an apomictic allopolyploid animal that we are aware of. This assembly should provide a very valuable framework for research into the diversity and functional divergence of plant pathogenic

nematode species. In the wider research landscape, genomes such as those from within the MIG can aid in our understanding of adaptation, ploidy, and evolution of genomes following hybridisation events and loss of meiosis [37].

Results

Sequencing and profiling of read libraries

We used PacBio single-molecule real-time (SMRT) sequencing technology, Hi-C chromatin conformation capture, Nanopore long-read sequencing, and Iso-Seq RNA sequencing to generate a genome assembly of *Meloidogyne javanica* strain VW4. Following quality control and concatenation of two libraries, we obtained 2,255,922 PacBio HiFi reads totalling 35.39 gbp (ACC: XXXXXX; S1 Fig). After quality control and concatenation of Oxford Nanopore PromethION data, we obtained 340,373 reads totalling 17.52 gbp (ACC: XXXXXX) (S2 Fig). Our Hi-C library contained 375,330,537 read pairs, of which 26.20% were of sufficiently high quality for scaffolding with *Proximo* (Phase Genomics, WA) (ACC: XXXXXX). After demultiplexing of our Iso-Seq library, we obtained 2,506,897 full-length non-chimeric sequences which collapsed into 59,637 high quality isoforms (ACC: XXXXXX).

Genome-wide k-mer profiling of concatenated PacBio HiFi read libraries with *smudgeplot* [38] indicated that 48% of the genome was tetraploid, 22% was triploid, and 29% was diploid (Fig 1A). However, this analysis likely underestimates the proportion of tetraploid regions, as crossover events or conversion between subgenomic copies can cause homogenisation. An incomplete or hypo-tetraploid state was also indicated using a k-mer spectra approach by *GenomeScope2*, predicting a haploid genome length of 68 mbp,

147 and a duplication rate of 3.4 [38] (Fig. 1B). This duplication rate is similar to the value seen

148 for CEGMA genes in other assemblies of *M. javanica* (3.68) [28].

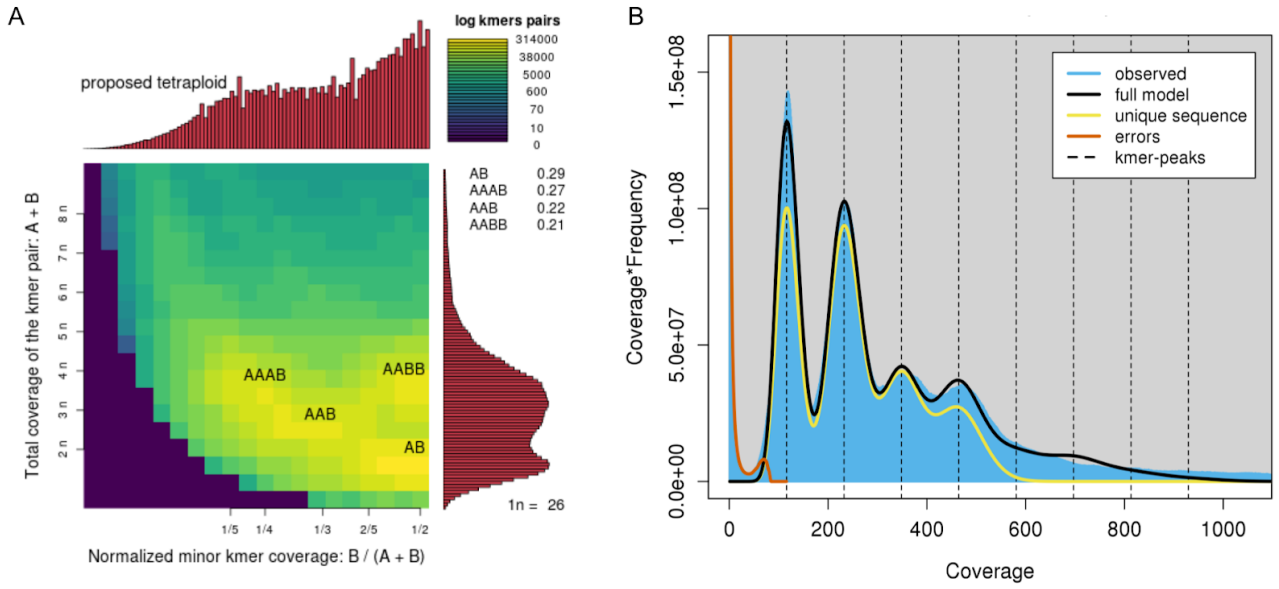

149

150 **Fig 1: Genome profiling plots.**

151 (A) Smudgeplot (left) proposing M. javanica as tetraploid, reporting the predicted

152 percentages of ploidy levels in the genome as follows: tetraploid (48%), triploid (22%), or

153 diploid (29%). (B) GenomeScope2 plot (right) showing four distinct peaks in both the

154 predicted model of tetraploidy (black line) and in the observed k-mer spectra (blue fill). The

155 amount of unique sequence falls to zero shortly after the fourth peak, indicating that k-mers

156 at higher ploidies than four were mostly repetitive elements.

157

158 # Assembly and annotation

159 ## Scaffolding and final assembly

160 From our draft assemblies of the PacBio data, we carried forward an iteration

161 assembled using *HiFiasm* [39] based on overall contiguity and comparison to expected

162 diploid genome length. Following purging of duplicates from the PacBio assembly and

163 scaffolding with Oxford Nanopore reads, we obtained 37 contigs with the N50 of 9.5 mbp.

164 Hi-C scaffolding with the *Proximo* pipeline identified 16 chromosome level clusters (Phase

165 Genomics Ltd), but increased the total number of scaffolds from 37 to 66. Following
166 scaffolding with Hi-C, *samba* [40] joined some small scaffolds and fragmented the largest
167 scaffold in the assembly, increasing the number of scaffolds from 66 to 69.

168 The final assembly scaffolds contains 150,545,692 bp with an N50 of 5,793,182 bp,
169 at 30.11% GC content, and overall, 99.96% of reads in our combined PacBio HiFi library
170 map successfully back to the assembly, indicating a high level of completeness (S1 Table).
171 Of the total assembly, 97.87% was contained in the longest 33 scaffolds (S3 Fig), which
172 ranged from 898 kbp to 9,595 kbp in length (Fig 2A; S6 Table). These 33 scaffolds
173 contained 99.85% of all transcribed gene models. Of the remaining 36 scaffolds, 4 were
174 identified by *blobtools* [41] as likely contaminants (Arthropoda, Chordata, and Streptophyta;
175 S4 Fig). One further contig was the *M. javanica* mitochondrial genome (Scaffold 67). The
176 remaining 31 small contigs were all less than 215 kbp, with a mean length of 88.9 kbp, and
177 since they contained few identifiably functional elements (0.19% of gene models), we
178 excluded them from the final analysis.

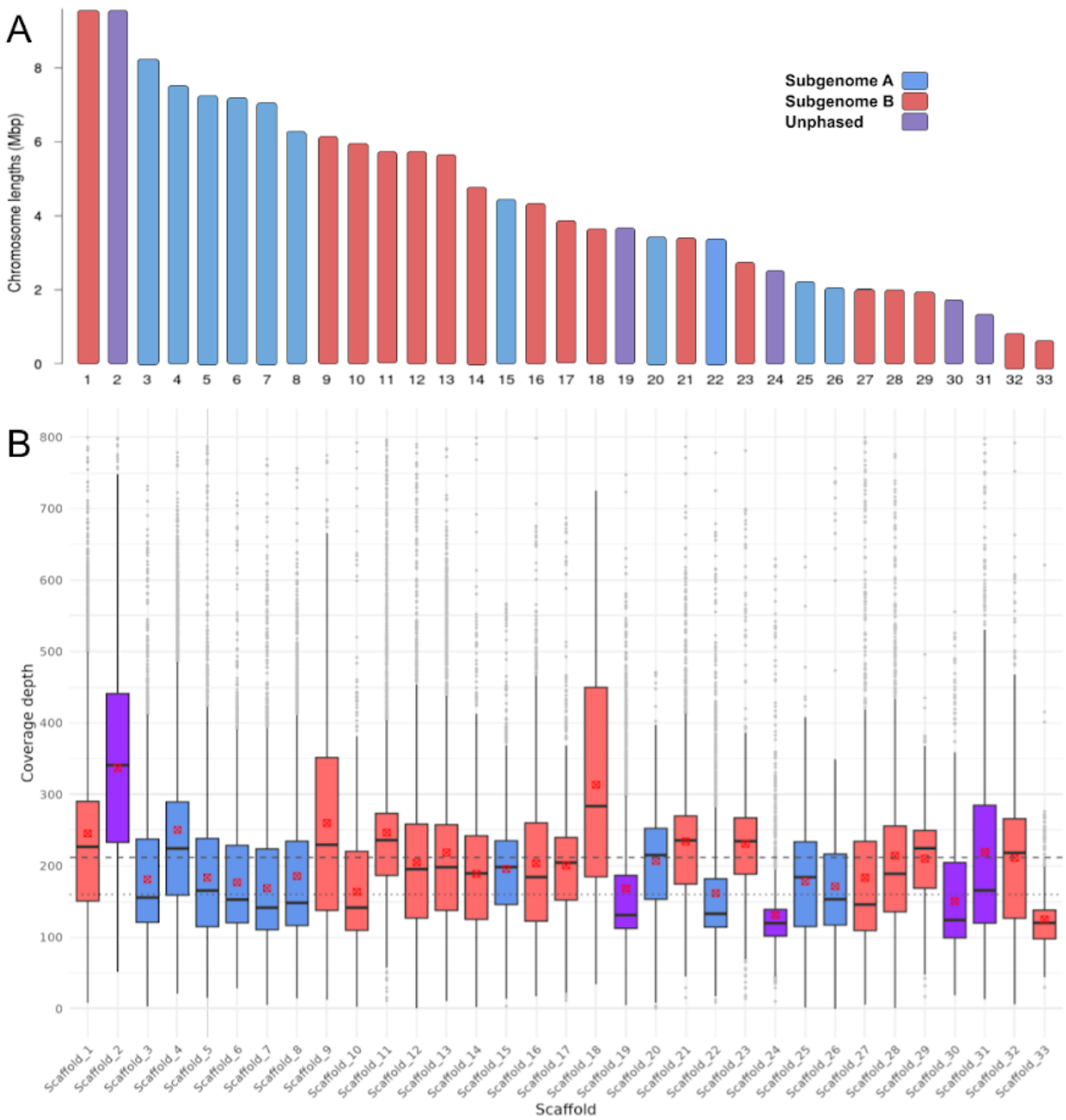

Fig 2. Ideogram and coverage depth of longest 33 scaffolds.

Scaffolds are coloured according to phasing status; blue - subgenome A, red - subgenome B, purple - unphased. A, Ideogram of 33 largest scaffolds. These 33 scaffolds contain 98% the total length of the assembly, with the remaining 36 contigs being shorter than 250 kbp, containing few gene models (0.19%), and consisting of mostly repetitive elements. B, Boxplot displaying the distribution of coverage depth for each scaffold. Red points denote the mean of data in each box. Coverage has been limited to a maximum of 800x to exclude probable repetitive sites with anomalous coverage depth. Dashed line shows the overall

188 mean for all coverage levels across 33 scaffolds. Dotted line shows the mode of all
189 coverage across 33 scaffolds.
190

191 ## Repeat annotation

192 In total 30.46% of our assembly was identified as repetitive elements, with 4.94%
193 identified as retroelements, 3.77% as DNA transposons, while 16.88% remain unclassified
194 repeats (S2 Table). A total of 164,394 transcripts, representing 59,632 isoforms, were
195 detected through mapping of our Iso-Seq library. *MAKER3* detected a total of 22,433
196 genes, containing 227,617 exons, 10,044 5' and 5,253 3' UTRs (S3 Table).

197 ## Core Eukaryotic Gene and Single Universal Copy Ortholog Analysis

198 Analysis of the final assembly with *CEGMA[42]* detected 233 of 248 CEGMA genes
199 (93.95%). This is a higher level of completeness than the most recent *M. javanica*
200 assembly, and comparable with contemporary *Meloidogyne* assemblies [19,36,43,44]

201 The average number of orthologs for each complete CEGMA gene (a proxy for
202 ploidy) is 1.88 indicating that only ~6% of the diploid genome is unassembled or not present
203 in the biological chromosomes. 173 complete BUSCO genes were detected, representing
204 67.9% of genes in the BUSCO eukaryote database. Of the BUSCOs identified, 31.4% were
205 duplicated (S5 Fig).

206

207 # Coverage and ploidy analysis

208 Mean coverage depth for all scaffolds - excluding mitochondrial - was 206.6x, falling
209 to 206.1x for the longest 33 scaffolds (Fig 2B). For some scaffolds (2, 9 and 18) coverage
210 depth was significantly in excess of this average, indicating collapsed regions; that is,
211 representation of three or four rather than two copies. Collapse is expected to arise in a
212 polyploid assembly when homoeologous sequences are similar enough at a nucleotide
213 level that they are inferred to be multiple homologous alleles of the same region, which are

214 then collapsed to form the reference assembly copy [8]. Other scaffolds (19, 22, 24, 33)
215 were underrepresented suggesting that they may be present as a single copy.

216 We then examined the coverage depth frequency distribution for each scaffold (Sup
217 Fig 7). For phased scaffolds representing two identical homologs, the frequency of
218 coverage for all bases in each scaffold would be expected to have a single peak (240x).
219 However, while predominantly single peaks were seen for under-represented scaffolds
220 thought to be present as a single copy (19, 22, 24, 33), we observed two peaks for the
221 majority of scaffolds (Fig 3A & C; S7 Fig). Two peaks would be expected if homologs are
222 not identical and similarity is disrupted by indels, with the second peak representing the
223 reduced coverage of the hemizygous region (~120x). For scaffold 2, which is over-
224 represented in coverage depth, four clear peaks are present (Fig 3) indicating that more
225 than two copies map to the scaffold. This likely resulted from exclusion of the scaffold's
226 homoeolog from the assembly, leading to an assembly collapse as noted above.
227 Nevertheless, the presence of 4 peaks is consistent with the presence of polymorphisms
228 between homologous copies as well as between homoeologous pairs.

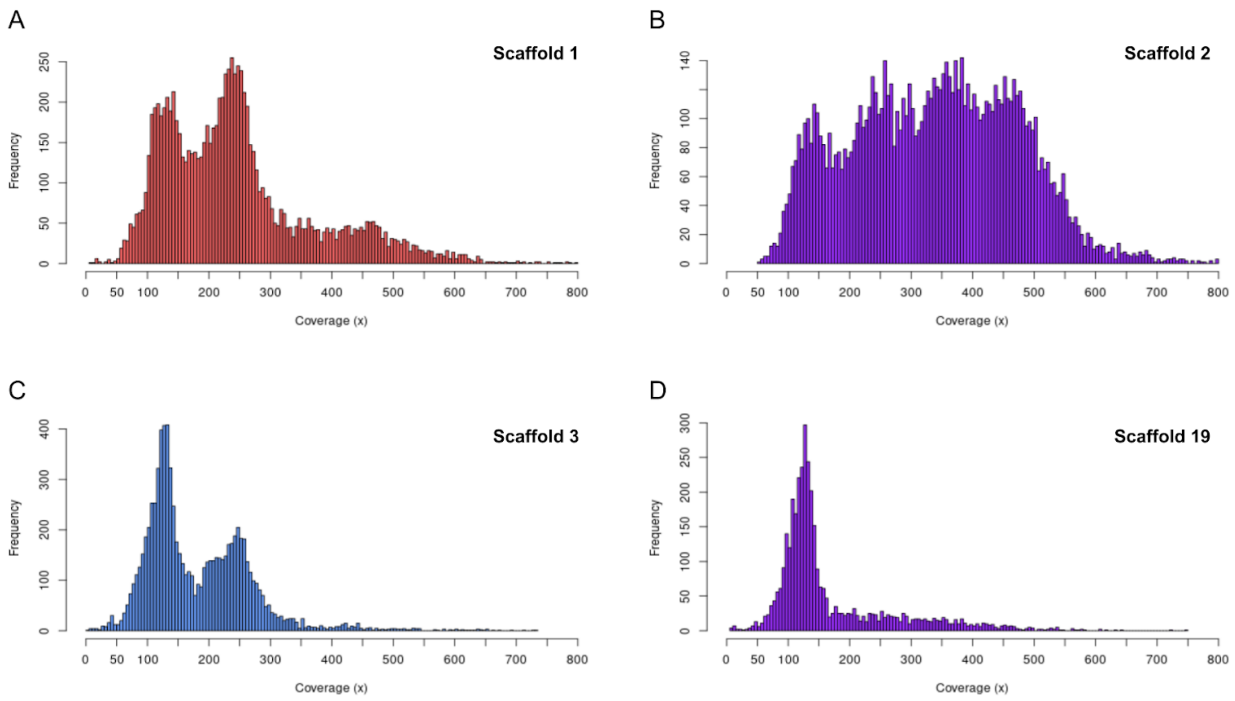

229

230 **Fig 3. Coverage depth frequency distributions of scaffolds 1, 2, 3, and 19.**

231 X-axis represents coverage depth and y-axis represents frequencies of coverage. Colour
232 indicates phase status: red for subgenome B, blue for subgenome A, and purple for
233 unphased scaffolds. (A) Scaffold 1, top left, displays two main peaks of coverage with a
234 small tail suggesting short collapsed regions. (B) Scaffold 2, top right, displays four peaks of
235 coverage, indicating that much of this scaffold is collapsed and four copies are mapping to
236 it. (C) Scaffold 3, bottom left, shows two peaks and very little tail, indicating two copies
237 mapping and little to no assembly collapse. (D) Scaffold 19, bottom right, shows only one
238 peak at ~120x coverage, suggesting that only one copy maps to this scaffold.

239

240 To examine the ploidy distribution in another way, we plotted a sliding window of
241 coverage across each scaffold (S8 Fig). In support of the coverage depth distributions, the
242 most frequent outcome was that scaffolds in the assembly show two layers of stratification
243 in coverage at a constant proportional depth, indicating two copies distinguished by indels
244 between them. This pattern was strongest for scaffolds with two coverage peaks,
245 particularly phased homoeologs (discussed below, Fig. 3 A & B; S7 Fig). Scaffold 2 and
246 scaffold 18, which are over-represented in sequence depth, contain regions of four levels of
247 coverage depth covering much of the length of both (Fig 3B; S8a and 8d Figs). This
248 increased amount of stratification at proportionally higher coverage depths (360x and 480x)
249 reveals assembly collapse, where four copies map to a single site. Together these
250 coverage depth results suggest that the *M. javanica* assembly represents two
251 homoeologous subgenomes (~87% of total length), with only 13% of the assembly
252 unphased or collapsed.

253

254 # Identification of homoeologous pairs and phasing of
255 subgenomes

256 Given the diploid nature of the assembly, which represents each subgenome as a
257 single copy, we expected to find scaffolds from these subgenomes present in
258 homoeologous pairs. Through detection of shared orthologs (Supplementary Methods)
259 twenty pairings were identified between the longest 33 scaffolds of the assembly, each
260 sharing between 20 and 351 CDS orthologs (Fig 4, S4 Table). Alternative methods of
261 identifying homoeologous pairs were corroborative (S5 Table). Some pairs were not
262 mutually exclusive, and exhibited CDS links to scaffolds outside of the primary pair,
263 suggesting translocation and syntenic changes between them. All scaffolds that showed
264 two depths of coverage were assigned as homoeologous pairs as expected if each
265 subgenome was heterozygous. Four scaffolds were excluded from pairings including
266 scaffold 2 which showed high amounts of collapse and scaffolds 19, 24, 30, and 31 which
267 are relatively small and/or present as single copies (S7 Fig and 9; S6 Table).

268 In order to assign contigs to a subgenome, we used a modified version of an
269 ancestral k-mer spectra analysis [45] (Supplementary Methods). This approach is based on
270 the premise that the allopolyploid's subgenomes possess repeats that diverged in the two
271 parental genomes before hybridisation. This results in a distinguishable signature in each
272 subgenome's k-mer spectrum, and allows us to determine the parental species from which
273 a given sequence descends. We successfully phased 85.39% of the genome into A or B
274 subgenomes (Fig 2A; S9 Fig; S6 Table). Scaffold 2, which exhibits extensive assembly
275 collapse, did not phase using these methods. Some smaller scaffolds that did not phase by
276 k-mer based methods were later assigned to a subgenome based on the phase status of
277 their opposing homoeologous scaffold (S6 Table). Of the total length of the final assembly,
278 39.15% was assigned to subgenome A and 46.24% was assigned to subgenome B, leaving
279 only 14.61% unassigned.

Subgenomic synteny analysis

Comparison of annotation of scaffold pairs assigned to subgenomes A and B revealed both long regions of synteny and large structural differences between subgenomes (Fig 4). Scaffold 13 and scaffold 15 are syntenic along almost the entire length of the shorter homoeolog and share high nucleotide similarity throughout. Similarly, scaffold pairs 20 and 23, as well as 17 and 25, share long syntenic blocks of shared CDS and long runs of high nucleotide similarity.

Scaffolds 7 and 10 are syntenic for almost half of their length whilst the remaining sequence lengths share no synteny and have very low nucleotide similarity. Synteny analysis and scaffold comparison suggest that chromosomal fragmentation has occurred. For example, scaffold 8 of subgenome A shows long collinear blocks with scaffolds 16, 28, 29, and 33 of subgenome B. Re-examination of Hi-C and ONT long-read scaffolding as well as manual inspection of read mapping support this fragmentation. Scaffold 1 of subgenome B shares syntenic blocks with scaffolds 5, 6, and 8 of subgenome A, in an order that suggests chromosomal structural differences between the subgenomes. Many phased scaffolds also exhibit small amounts of extra-pair synteny indicating numerous small translocations throughout the genome.

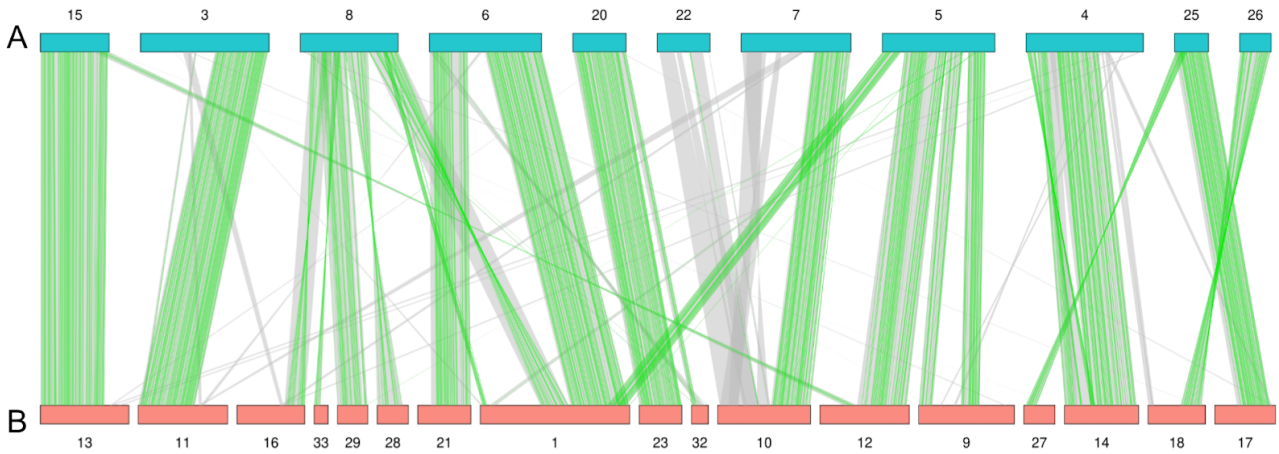

299 **Fig 4. Macrosynteny analysis between subgenomes.**

300 Glyphs along top and bottom represent scaffolds assigned to either subgenome A (blue) or
301 subgenome B (red). Green lines mark locations of synteny between transcribed genes
302 identified from mapping of Iso-Seq sequences. Grey lines mark locations of synteny
303 between genes identified through *MAKER3* gene prediction. Synteny and collinearity were
304 identified using the *MCScan* module of *JCVI* using Iso-Seq informed transcriptional
305 annotation. Scaffolds that could not be assigned to a subgenome are not shown.

306

307

308 Discussion

309 Assembly of the allopolyploid genome of *M. javanica*

310 We have used long-read sequencing and modern bioinformatic approaches to
311 assemble and phase the allopolyploid genome of the plant pathogenic nematode
312 *Meloidogyne javanica*. Our goal was to assemble a contiguous diploid assembly for *M.*
313 *javanica*, representing the A and B subgenomes separately. Our current diploid assembly
314 (150,545,692 bp) is, as expected for a tetraploid, approximately half the 297 ±27Mb
315 measured by flow cytometry [19,28]. This total length is representative of both A and B
316 subgenomes except for collapsed regions where sequence for both subgenomes A and B is
317 considered together. Because some regions of the assembly have been shown by k-mer
318 profiling and coverage analysis to be present in less than four copies (Fig 1; S8 Fig),
319 splitting the subgenomes into their component copies (A1, A2, B1, B2) to create a tetraploid
320 assembly would not be expected to completely double the length.

321 Annotation

322 We annotated our assembly using both *ab initio* feature prediction algorithms and
323 mapping of the full-length transcript sequences (S3 Table). The total number of genes

predicted - 22,433 - is within the range expected for a MIG species and is comparable to previous *M. javanica* assemblies [19,28].

BUSCO scores for *Meloidogyne* are consistently lower than those of more widely studied organisms, and the number of genes we have detected (S3 Table) in the genome is consistent with what has been found for other *Meloidogyne* species [19,28,46]. The paucity of established protein databases for less frequently investigated genera limits the accuracy of prediction-based annotation methods. Loss of core genes are not unexpected for this group of highly specialised, obligate parasites. With increased availability of sequence resources for plant parasitic nematodes, it should soon be possible to develop a more appropriate set of core genes.

Evidence for a chromosome-scale assembly

Previous genomic assemblies of *M. javanica* have contig counts numbering in the thousands [19,28]. In our current assembly, more than 99% of reads in our PacBio HiFi libraries map to 33 large scaffolds (Fig 2B). We propose that most of the 33 scaffolds represent full-length or nearly full-length chromosomes. Cytological examination in *M. javanica* indicates that the chromosome number ranges from 42-48 due to variation between isolates (Eisenback and Triantaphyllou, 1991; Triantaphyllou 1985, Janssen et al 2017). Thus, we would expect 21-24 scaffolds in our assembly. The discrepancy between scaffold number and cytological observations could be due to an imperfect assembly or failure to identify very small chromosomes in the cytological studies. We have employed several independent scaffolding softwares, Hi-C chromatin contact mapping, and the manual examination of long-read mapping to contig termini, and see no evidence to support fusing additional contigs. Additional molecular and cytological studies may be required to resolve these differences.

Many chromosome-scale assemblies identify telomeres as defining the range of their scaffolds, yet we did not identify canonical telomeric repeats at scaffold termini.

350 Additionally, we were also not able to identify a homolog of *C. elegans* telomerase (*trt-1;*
351 ACC: NM_001373211.4) in our assembly. This may suggest that non-standard telomere
352 processes might be operating in root-knot nematodes as has been found for fruit flies
353 [49,50].

354

355 Genetic variation in *M. javanica* is dominated by indels

356 We present the assembly as a diploid representation. Read depth analysis of
357 individual scaffolds indicates that homologs are not identical and indels are frequent.
358 Additionally some scaffolds appear to be present as a single copy suggesting that one of
359 the homologs may have been lost. We identified many indels that delete or disrupt one or
360 more copies of coding sequences, indicating that *M. javanica* is no longer genome-wide
361 tetraploid either in copy number or functionality. A higher propensity for indel accumulation
362 has been frequently seen in hybrid parthenogenetic species [51] and partial return to lower
363 ploidy is a characteristic of many polyploids.

364 We find that 87% of our diploid assembly consists of one copy of either subgenome
365 in homoeologous pairs, with two copies mapping to phased scaffolds and four copies
366 mapping to collapsed regions. We successfully phased much of our assembly into
367 subgenomes using k-mer signatures, enabling for the first time initial genome-wide
368 comparison of MIG A and B subgenomes. Some scaffolds, notably scaffold 2 and some of
369 the short scaffolds, could not be assigned to subgenomes. Scaffold 2 displays four levels of
370 stratification in its coverage (S8 Fig) and four peaks in its depth distribution (Fig 3b)
371 indicating that the four copies (A1+A2 and B1+B2) are almost entirely collapsed into a
372 single scaffold. We suggest that the homoeologous chromosomes represented by scaffold
373 2 may be too similar in sequence to assign to a subgenome by k-mer analysis due to a
374 possible homogenization event. For the smaller scaffolds, the failure may have been due to
375 their small size because they did not contain enough relevant k-mers. Some of the small

376 scaffolds were later assigned to a subgenome using transcript alignments. No misassembly
377 or erroneous scaffolding of the unphased sequences was detected through either
378 programmatic or manual methods.

379 The allotetraploid genome of *M. javanica* demonstrates extensive synteny between
380 the A and B subgenomes with most genic regions represented in four copies. We would
381 expect however that there would be differences between the subgenomes, including indels
382 and other structural variation, as this is typically observed between different species and the
383 MIG have a hybrid origin. In accordance with this, we observed very substantial structural
384 variation between subgenomes A and B, including insertions, deletions, and translocations
385 (Fig 4).

386

387 Loss of synteny and fragmentation

388 We observe regions of the *M. javanica* genome where synteny between paired
389 chromosomes is disrupted. One reason for this could be that the parental species (A and B)
390 had genomes in which the non-syntenic regions had diverged by translocation, insertion or
391 deletion. Upon hybridisation to create the allopolyploid MIG these diverged regions form the
392 end of synteny blocks. An alternative explanation is that these changes happened after the
393 hybridisation event in the tumultuous process of genome stabilisation immediately following
394 it [52,53]. Hybridisation, polyploidization, and the loss of meiosis are processes often
395 associated with rapid genomic change [54][51,54,55] and the unique MIG species
396 allopolyploid genomes we are currently studying may represent different balances between
397 these forces. We observe 11 chromosome-scale scaffolds in subgenome A and 17 in
398 subgenome B despite the clear synteny throughout these two genomes. Several scaffolds
399 in subgenome A contain blocks of genes with regions that are syntenic to different
400 subgenome B scaffolds. Similarly, there are cases where syntenic blocks in subgenome B
401 are present on different scaffolds in subgenome A. Together these differences suggest that

402 ancestral chromosomal fission, or fusion events or other types of exchange have occurred.
403 *Meloidogyne* species, like other nematodes, have holocentric chromosomes
404 (Triantaphyllou, 1985). Genomes with dispersed centromere structure are predicted to
405 better tolerate chromosome fragmentation and fusion [56], as are species with ameiotic
406 mechanisms of reproduction. The observed differences in copy number of chromosomes
407 between isolates of *M. javanica* may be additional evidence for tolerance of chromosome
408 fragmentation/fusion. Although it is always necessary to consider the possibility of
409 misassembly or rogue scaffolding, we have substantial evidence through manual inspection
410 and contiguous mapping of ultra-long Oxford Nanopore reads that our assembly is correct.

411 The majority of published assemblies of allopolyploids come from plants, where
412 polyploidy might have shaped the genomes of around 70% of species [57]. Many
413 allopolyploid plant genomes, however, show a higher level of synteny and structural
414 conservation than we observe for *M. javanica* [13,45,58]. Similarly the few available
415 chromosomal allopolyploid animal genome sequences available [14,15] do not show
416 extensive deletions and chromosomal fissions as does our genome. Unlike other
417 allopolyploid species with chromosomal genome sequences, *Meloidogyne javanica*
418 reproduces by obligatory mitotic parthenogenesis (apomixis) and this lack of meiotic
419 chromosome pairing may allow greater structural divergence and tolerance for the decay of
420 synteny. We note that genomes from species not able to reproduce by meiosis are currently
421 rare [51] and suggest that much more substantial genomic work on a range of species with
422 different reproductive modes and ploidy levels will be required to reveal the diverse
423 mechanisms shaping these genomes. It is apparent however that the changes surrounding
424 allopolyploidy have contributed to the gene content, heterozygosity, and copy number
425 throughout the *M. javanica* genome and these processes of locally fixed heterozygosity or
426 rediploidization may contribute extensively to adaptive functional variation [59].

427

428 ## Regional homogenization of subgenomes

429 Some regions of the genome do not phase into A and B homoeologs due to very low
430 divergence between the four gene copies. This could be explained either by the loss of
431 whole chromosomes, compensated by the duplication of the remaining chromosome, or
432 mitotic recombination (gene conversion) between homoeologs [60,61]. It is unclear from
433 this single genome how asexual recombination contributes to shaping the diversity of *M.*
434 *javanica*, however this has been suggested in previous MIG genomic studies [19,28] and
435 may be further elucidated by our ongoing molecular evolution and population genomic
436 studies.

437 The initial tetraploidy of *M. javanica* will buffer against deleterious phenotypic
438 consequences of indels, allowing a substantial accumulation of genetic variation by this
439 mechanism. It has been argued for angiosperms that this rediploidization process can
440 contribute to adaptive species divergence by providing genomic and transcriptomic diversity
441 [59,62]. Other mechanisms of adaptive divergence may also operate at the same time. The
442 increase in gene copy number created by polyploidization gives the potential for functional
443 gene divergence by neo- or sub-functionalization, as well as adaptive phenotypes driven by
444 copy number loss [63–65]. Adaptation by gene copy number variation has already been
445 reported in *M. incognita* [66] and it may be that genomic copy number variation more
446 broadly is a major source of functional genetic variation in the MIG.

447

448 ## A genomic framework for RKN functional and diversity studies

449 In this paper we present a highly contiguous, annotated and phased genome of the
450 allotetraploid plant pathogenic nematode *M. javanica*. This genome assembly will provide
451 many tools for diverse investigations by plant pathologists and nematologists in addition to
452 adding to our understanding of the origins and diversity of *M. javanica*. It will also serve as a

453 reference for investigating genome structure and pathogenicity in other *Meloidogyne*
454 species.

455 The contiguous nature of this genome and the high quality annotation will facilitate
456 RKN functional studies since transcripts can be mapped accurately to the annotated
457 subgenome. This allows consideration of copy number variation, which may be an
458 important component of functional variation in these species.

459 Progress is being made by many groups in understanding the basis of nematode
460 virulence and the key loci involved [67–69]. In such cases even light coverage sequencing
461 of field isolates mapped to a high quality genome could give valuable information to
462 commercial growers about the likely pathogenicity of those strains [70].

463

464

465 # Methods

466 ## Reproducibility

467 Wherever possible, this study attempted to contain all bioinformatic processes in
468 reproducible workflows or scripts, for the purpose of openness and enabling replication.
469 Workflows and code are archived in a Zenodo repository along with final outputs
470 (doi://XXXXXX.XX). The raw reads plus final nuclear and mitochondrial assemblies are
471 available on the International Nucleotide Sequence Databases (INSDC) (ACC: XXXXXX)
472 (ACC: XXXXXX).

473

474 # Biological material

475 *Meloidogyne javanica* strain VW4 was used for this work (Gleason et al, 2008;
476 Szitenberg et al., 2017). Cultures of this strain have been maintained on tomato plants
477 under greenhouse conditions for over 30 years (Yaghoobi et al, 1995). Periodic transfers of
478 single egg masses have been carried out to maintain uniformity. For DNA preparation, eggs
479 were harvested from roots and cleaned by sucrose flotation as previously described
480 (Branch et al, 2004) then flash-frozen in liquid N2. High molecular weight DNA (HMW DNA)
481 isolation was carried out at UC Davis Genome Center (Supplementary Methods). Integrity
482 of the HMW gDNA was verified on a Femto Pulse system (Agilent Technologies, CA) where
483 majority of the DNA was found to be in fragments above 100 Kb.

484 Total RNA was isolated from three *M. javanica* life stages: eggs, freshly hatched
485 juveniles, and females dissected from tomato roots 21 days after infection. This material
486 was flash-frozen and RNA was extracted using an RNeasy Kit (Qiagen, USA) following the
487 manufacturer's instructions. TURBO DNase treatment was carried out to remove genomic
488 DNA from total RNA samples (TURBO DNA-free Kit™, Ambion, USA). RNA concentration
489 and purity were measured using a NanoDrop OneC Microvolume UV-Vis
490 Spectrophotometer (Thermo Scientific, USA). RNA integrity and quality was assessed using
491 bioanalyzer.

492

493 # Sequencing and QC

494 ## High fidelity (HiFi) long-read sequencing

495 PacBio HiFi library preparation and sequencing of HMW DNA was performed by UC
496 Davis DNA Technologies Core on a PacBio Sequel II (Supplementary Methods). Data from
497 the two generated libraries were pooled and only reads longer than 5000 bp and with a
498 quality score over 15 were retained.

499 ## Nanopore sequencing

500 Nanopore sequencing of HMW DNA using Oxford Nanopore Technologies (ONT)
501 systems was carried out by UC Davis DNA Technologies Core. The super-long-read DNA
502 sequencing protocol (Supplementary Methods) yielded 23 gbp of data, which was then
503 filtered to contain only reads longer than 25 kbp.

504 ## Hi-C chromatin conformation capture

505 DNA was prepared using Proximo Hi-C kit (Animal) as recommended by the
506 manufacturer (Phase Genomics, Seattle, WA, USA). Library preparation and sequencing
507 were carried out at the UC Davis DNA Technologies Core and scaffolding with Proximo was
508 performed by Phase Genomics (Supplementary Methods).

509 ## PacBio Iso-Seq

510 Reads from one Sequel II SMRT cell were quality controlled and converted into
511 clustered reads using the *IsoSeq3* pipeline with default parameters [71].

512

513 # Genome profiling

514 Profiling was performed by *Genomescope2* and *smudgeplot [38].* All quality
515 controlled PacBio HiFi libraries were combined and used as input for these programs. Both
516 were run with default parameters, aside from *-ploidy* in *Genomescope2* set to 4, as this was
517 the primary ploidy indicated by *smudgeplot* and suggested by visual analysis of mapped
518 reads.

519

Assembly

Draft assembly

Initial draft assemblies were generated using several different assemblers and appraised with *asmapp [72].* The most appropriate assembly based on length and contiguity was carried forward, after which haplotigs were identified and removed using *purge_dups* [73].

Scaffolding with Oxford Nanopore and Hi-C

We used *SLR* [74] to scaffold the assembly with our trimmed and concatenated ONT reads. The assembly was then scaffolded with Hi-C reads using the *Proximo* pipeline by Phase Genomics Ltd. The resulting contact map was manually curated using *Juicebox* assembly tools [75] to produce the most likely assembly based on contact linkage information and TAD presence or absence. A third phase of scaffolding was performed by *samba,* to break potential misassemblies introduced during manual *Juicebox* scaffolding and scaffold sequences that were broken as debris [40].

Annotation

Repeat annotation

RepeatModeler was applied to the assembly [76], with the resulting library of repeat models used as input for *RepeatMasker* to annotate repeat regions and generate a soft-masked version of the genome [77].

Gene annotation

Iso-Seq reads were mapped to the genome and collapsed using a *snakemake* workflow automating the *IsoSeq3* pipeline [71]. The annotation pipeline *MAKER3* was then

543 employed to perform *ab initio* and predictive annotation of our genome [78,79]. Full
544 methods of annotation iterations and parameters can be found in Supplementary Methods.

545

546 Subgenome phasing

547 Identification of homoeologous scaffold pairs

548 Homoeologous pairs were detected through identification of orthologs shared
549 between scaffolds (Supplementary Methods). Pairs sharing a large number of orthologs
550 and nucleotide similarity were considered homoeologous. This was validated with other
551 methods, including MASH distance [80] and shared possession of duplicated BUSCO
552 genes [81].

553 Phasing of subgenomes

554 Scaffolds were phased into A and B subgenomes using a k-mer-based approach
555 built on the approach taken by [45]. K-mers in the assembly were detected and counted
556 using *jellyfish[82]*, with only k-mers present more than 75 times in the assembly and
557 represented at least twice as often in one subgenome than the other carried forward. These
558 counts were then transformed into binomial distributions. Hierarchical clustering was
559 performed on these sets, creating a dendrogram placing scaffolds into opposing clusters,
560 each cluster representing a subgenome (Supplementary Methods).

561

562 Synteny analysis

563 The *MCScan (Python)* [83] module of *JCVI [84]*was used to perform a synteny
564 analysis between the two subgenomes. Custom scripts then extracted collinearity
565 information and generated synteny plots (Supplementary Methods).

566

567

568 # Acknowledgments

569 We acknowledge the Viper High Performance Computing facility of the University of
570 Hull and its support team, specifically Chris Collins, for their invaluable help in managing
571 and deploying software, as well as the high Performance Computing team at UC Davis for
572 making available their resources for part of our analysis.

573

574

575 # References

576 1. Glover NM, Redestig H, Dessimoz C. Homoeologs: What Are They and How Do We
577 Infer Them? Trends Plant Sci. 2016;21: 609–621. doi:10.1016/j.tplants.2016.02.005

578 2. Barker MS, Arrigo N, Baniaga AE, Li Z, Levin DA. On the relative abundance of
579 autopolyploids and allopolyploids. New Phytol. 2015. doi:10.1111/nph.13698

580 3. Schoenfelder KP, Fox DT. The expanding implications of polyploidy. J Cell Biol.
581 2015;209: 485–491. doi:10.1083/jcb.201502016

582 4. Session AM, Uno Y, Kwon T, Chapman JA, Toyoda A, Takahashi S, et al. Genome
583 evolution in the allotetraploid frog Xenopus laevis. Nature. 2016;538: 336–343.
584 doi:10.1038/nature19840

585 5. Ming R, Man Wai C. Assembling allopolyploid genomes: no longer formidable.
586 Genome Biol. 2015;16: 27. doi:10.1186/s13059-015-0585-5

587 6. Kyriakidou M, Tai HH, Anglin NL, Ellis D, Strömvik MV. Current Strategies of
588 Polyploid Plant Genome Sequence Assembly. Front Plant Sci. 2018;9: 1660.
589 doi:10.3389/fpls.2018.01660

590 7. Rhie A, McCarthy SA, Fedrigo O, Damas J, Formenti G, Koren S, et al. Towards
591 complete and error-free genome assemblies of all vertebrate species. Nature. 2021;592:
592 737–746. doi:10.1038/s41586-021-03451-0

593 8. Zhang X, Wu R, Wang Y, Yu J, Tang H. Unzipping haplotypes in diploid and
594 polyploid genomes. Comput Struct Biotechnol J. 2020;18: 66–72.
595 doi:10.1016/j.csbj.2019.11.011
596 9. Saada OA, Friedrich A, Schacherer J. Towards accurate, contiguous and complete
597 alignment-based polyploid phasing algorithms. Genomics. 2022;114: 110369.
598 doi:10.1016/j.ygeno.2022.110369
599 10. Edger PP, Poorten TJ, VanBuren R, Hardigan MA, Colle M, McKain MR, et al. Origin
600 and evolution of the octoploid strawberry genome. Nat Genet. 2019;51: 541–547.
601 doi:10.1038/s41588-019-0356-4
602 11. Gan X, Li S, Zong Y, Cao D, Li Y, Liu R, et al. Chromosome-Level Genome
603 Assembly Provides New Insights into Genome Evolution and Tuberous Root
604 Formation of Potentilla anserina. Genes . 2021;12. doi:10.3390/genes12121993
605 12. Kolesnikova UK, Scott AD, Van de Velde JD, Burns R, Tikhomirov NP, Pfordt U, et
606 al. Genome of selfing Siberian Arabidopsis lyrata explains establishment of
607 allopolyploid Arabidopsis kamchatica. bioRxiv. 2022. p. 2022.06.24.497443.
608 doi:10.1101/2022.06.24.497443
609 13. Zheng Y, Yang D, Rong J, Chen L, Zhu Q, He T, et al. Allele-aware chromosome-
610 scale assembly of the allopolyploid genome of hexaploid Ma bamboo
611 (Dendrocalamus latiflorus Munro). J Integr Plant Biol. 2022;64: 649–670.
612 doi:10.1111/jipb.13217
613 14. Du K, Stöck M, Kneitz S, Klopp C, Woltering JM, Adolfi MC, et al. The sterlet
614 sturgeon genome sequence and the mechanisms of segmental rediploidization.
615 Nature Ecology & Evolution. 2020;4: 841–852. doi:10.1038/s41559-020-1166-x
616 15. Kuhl H, Du K, Schartl M, Kalous L, Stöck M, Lamatsch DK. Equilibrated evolution of
617 the mixed auto-/allopolyploid haplotype-resolved genome of the invasive hexaploid
618 Prussian carp. Nat Commun. 2022;13: 4092. doi:10.1038/s41467-022-31515-w

619 16. Perry RN, Moens M, Starr JL. Root-knot Nematodes. CABI; 2009. Available:
620 https://play.google.com/store/books/details?id=UN3uHMr_UCoC
621 17. Williamson VM, Gleason CA. Plant–nematode interactions. Curr Opin Plant Biol.
622 2003;6: 327–333. doi:10.1016/S1369-5266(03)00059-1
623 18. Trudgill DL, Blok VC. Apomictic, polyphagous root-knot nematodes: exceptionally
624 successful and damaging biotrophic root pathogens. Annu Rev Phytopathol.
625 2001;39: 53–77. doi:10.1146/annurev.phyto.39.1.53
626 19. Szitenberg A, Salazar-Jaramillo L, Blok VC, Laetsch DR, Joseph S, Williamson VM,
627 et al. Comparative Genomics of Apomictic Root-Knot Nematodes: Hybridization,
628 Ploidy, and Dynamic Genome Change. Genome Biol Evol. 2017;9: 2844–2861.
629 doi:10.1093/gbe/evx201
630 20. Wesemael W, Viaene N, Moens M. Root-knot nematodes (Meloidogyne spp.) in
631 Europe. Nematology. 2011;13: 3–16. doi:10.1163/138855410X526831
632 21. Jones JT, Haegeman A, Danchin EGJ, Gaur HS, Helder J, Jones MGK, et al. Top 10
633 plant-parasitic nematodes in molecular plant pathology. Mol Plant Pathol. 2013;14:
634 946–961. Available:
635 https://bsppjournals.onlinelibrary.wiley.com/doi/abs/10.1111/mpp.12057
636 22. Bernard GC, Egnin M, Bonsi C. The impact of plant-parasitic nematodes on
637 agriculture and methods of control. Nematology-Concepts, Diagnosis and Control.
638 2017;10. Available:
639 https://books.google.co.uk/bookshl=en&lr=&id=MQWQDwAAQBAJ&oi=fnd&pg=PA1
640 21&dq=agricultural+impact+root-knot+nematodes&ots=bBkbCxpflc&sig=1tg90hY-
641 8Y2Z7V_6F8KGljCENoM

642 23. Eisenback JD, Triantaphyllou HH. Root-knot nematodes: Meloidogyne species and
643 races. Manual of agricultural nematology. 1991;1: 191–274. Available:
644 https://www.researchgate.net/profile/Jonathan_Eisenback/publication/
645 283548298_Root-Knot_Nematodes_Meloidogyne_Species_and_Races/links/
646 563e67e308ae34e98c4d93c1/Root-Knot-Nematodes-Meloidogyne-Species-and-
647 Races.pdf
648 24. Subbotin SA, Rius JEP, Castillo P. Systematics of Root-knot Nematodes (Nematoda:
649 Meloidogynidae). BRILL; 2021. Available:
650 https://play.google.com/store/books/details?id=xs87EAAAQBAJ
651 25. Triantaphyllou AC. Gametogenesis and the Chromosomes of Meloidogyne nataliei:
652 Not Typical of Other Root-knot Nematodes. J Nematol. 1985;17: 1–5. Available:
653 https://www.ncbi.nlm.nih.gov/pubmed/19294050
654 26. Bird DM, Williamson VM, Abad P, McCarter J, Danchin EGJ, Castagnone-Sereno P,
655 et al. The genomes of root-knot nematodes. Annu Rev Phytopathol. 2009;47: 333–
656 351. doi:10.1146/annurev-phyto-080508-081839
657 27. Lunt DH. Genetic tests of ancient asexuality in root knot nematodes reveal recent
658 hybrid origins. BMC Evol Biol. 2008;8: 194. doi:10.1186/1471-2148-8-194
659 28. Blanc-Mathieu R, Perfus-Barbeoch L, Aury J-M, Da Rocha M, Gouzy J, Sallet E, et
660 al. Hybridization and polyploidy enable genomic plasticity without sex in the most
661 devastating plant-parasitic nematodes. PLoS Genet. 2017;13: e1006777.
662 doi:10.1371/journal.pgen.1006777
663 29. Hartman KM, Sasser JN. Identification of Meloidogyne species on the basis of
664 differential host test and perineal pattern morphology. An advanced treatise on
665 Meloidogyne. 1985;2: 69–77. Available: https://books.google.com/books?
666 hl=en&lr=&id=gNo4AQAAIAAJ&oi=fnd&pg=PA69&dq=hartman+and+sasser&ots=r0
667 T3kOF2TR&sig=qp5-qepxxIy-MaZ3Yxq8q3OTlBg

668 30. Roberts PA, Thomason J. Variability in reproduction of isolates of Meloidogyne
669 incognita and M. javanica on resistant tomato genotypes. worldveg.tind.io; 1986.
670 Available: https://worldveg.tind.io/record/4772/
671 31. Rammah A, Hirschmann H. Morphological Comparison of Three Host Races of
672 Meloidogyne javanica. J Nematol. 1990;22: 56–68. Available:
673 https://www.ncbi.nlm.nih.gov/pubmed/19287689
674 32. Williamson VM, Kumar A. Nematode resistance in plants: the battle underground.
675 Trends Genet. 2006;22: 396–403. doi:10.1016/j.tig.2006.05.003
676 33. Gleason CA, Liu QL, Williamson VM. Silencing a candidate nematode effector gene
677 corresponding to the tomato resistance gene Mi-1 leads to acquisition of virulence.
678 Mol Plant Microbe Interact. 2008;21: 576–585. doi:10.1094/MPMI-21-5-0576
679 34. Hajihassani A, Marquez J, Woldemeskel M, Hamidi N. Identification of Four
680 Populations of Meloidogyne incognita in Georgia, United States, Capable of
681 Parasitizing Tomato-Bearing Mi-1.2 Gene. Plant Dis. 2022;106: 137–143.
682 doi:10.1094/PDIS-05-21-0902-RE
683 35. Sato K, Kadota Y, Gan P, Bino T, Uehara T, Yamaguchi K, et al. High-Quality
684 Genome Sequence of the Root-Knot Nematode Meloidogyne arenaria Genotype A2-
685 O. Genome Announc. 2018;6. doi:10.1128/genomeA.00519-18
686 36. Susič N, Koutsovoulos GD, Riccio C, Danchin EGJ, Blaxter ML, Lunt DH, et al.
687 Genome sequence of the root-knot nematode Meloidogyne luci. J Nematol. 2020;52:
688 1–5. doi:10.21307/jofnem-2020-025
689 37. Fox DT, Soltis DE, Soltis PS, Ashman T-L, Van de Peer Y. Polyploidy: A biological
690 force from cells to ecosystems. Trends Cell Biol. 2020;30: 688–694.
691 doi:10.1016/j.tcb.2020.06.006

692 38. Ranallo-Benavidez TR, Jaron KS, Schatz MC. GenomeScope 2.0 and Smudgeplot
693 for reference-free profiling of polyploid genomes. Nat Commun. 2020;11: 1432.
694 doi:10.1038/s41467-020-14998-3
695 39. Cheng H, Concepcion GT, Feng X, Zhang H, Li H. Haplotype-resolved de novo
696 assembly using phased assembly graphs with hifiasm. Nat Methods. 2021;18: 170–
697 175. doi:10.1038/s41592-020-01056-5
698 40. Zimin AV, Salzberg SL. The SAMBA tool uses long reads to improve the contiguity of
699 genome assemblies. PLoS Comput Biol. 2022;18: e1009860.
700 doi:10.1371/journal.pcbi.1009860
701 41. Laetsch DR, Blaxter ML. BlobTools: Interrogation of genome assemblies. F1000Res.
702 2017;6: 1287. doi:10.12688/f1000research.12232.1
703 42. Parra G, Bradnam K, Korf I. CEGMA: a pipeline to accurately annotate core genes in
704 eukaryotic genomes. Bioinformatics. 2007;23: 1061–1067.
705 doi:10.1093/bioinformatics/btm071
706 43. Koutsovoulos GD, Poullet M, El Ashry A, Kozlowski DK, Sallet E, Da Rocha M, et al.
707 The polyploid genome of the mitotic parthenogenetic root-knot nematode
708 Meloidogyne enterolobii. bioRxiv. 2019. p. 586818. doi:10.1101/586818
709 44. Kozlowski DKL, Hassanaly-Goulamhoussen R, Da Rocha M, Koutsovoulos GD,
710 Bailly-Bechet M, Danchin EGJ. Movements of transposable elements contribute to
711 the genomic plasticity and species diversification in an asexually reproducing
712 nematode pest. Evol Appl. 2021;14: 1844–1866. doi:10.1111/eva.13246
713 45. Cerca J, Petersen B, Lazaro-Guevara JM, Rivera-Colón A, Birkeland S, Vizueta J, et
714 al. The genomic basis of the plant island syndrome in Darwin's giant daisies. Nat
715 Commun. 2022;13: 3729. doi:10.1038/s41467-022-31280-w

716 46. Koutsovoulos GD, Poullet M, Elashry A, Kozlowski DKL, Sallet E, Da Rocha M, et al.
717 Genome assembly and annotation of Meloidogyne enterolobii, an emerging
718 parthenogenetic root-knot nematode. Scientific Data. 2020;7: 324.
719 doi:10.1038/s41597-020-00666-0
720 47. Koutsovoulos GD, Marques E, Arguel M, Duret L, Machado ACZ, Carneiro RMDG,
721 et al. Population genomics supports clonal reproduction and multiple independent
722 gains and losses of parasitic abilities in the most devastating nematode pest. Evol
723 Appl. 2019;26: 909. doi:10.1111/eva.12881
724 48. Bali S, Hu S, Vining K, Brown C, Mojtahedi H, Zhang L, et al. Nematode genome
725 announcement: Draft genome of Meloidogyne chitwoodi, an economically important
726 pest of potato in the pacific northwest. Mol Plant Microbe Interact. 2021;
727 MPMI12200337A. doi:10.1094/MPMI-12-20-0337-A
728 49. Mason JM, Reddy HM, Frydrychova RC. Telomere Maintenance in Organisms
729 without Telomerase. In: Seligmann H, editor. DNA Replication. Rijeka: IntechOpen;
730 2011. doi:10.5772/19348
731 50. Pardue M-L, DeBaryshe PG. Retrotransposons that maintain chromosome ends.
732 Proc Natl Acad Sci U S A. 2011;108: 20317–20324. doi:10.1073/pnas.1100278108
733 51. Jaron KS, Bast J, Nowell RW, Ranallo-Benavidez TR, Robinson-Rechavi M,
734 Schwander T. Genomic Features of Parthenogenetic Animals. J Hered. 2021;112:
735 19–33. doi:10.1093/jhered/esaa031
736 52. Edger PP, McKain MR, Bird KA, VanBuren R. Subgenome assignment in
737 allopolyploids: challenges and future directions. Curr Opin Plant Biol. 2018;42: 76–
738 80. doi:10.1016/j.pbi.2018.03.006

739 53. Emery M, Willis MMS, Hao Y, Barry K, Oakgrove K, Peng Y, et al. Preferential
740 retention of genes from one parental genome after polyploidy illustrates the nature
741 and scope of the genomic conflicts induced by hybridization. PLoS Genet. 2018;14:
742 e1007267. doi:10.1371/journal.pgen.1007267
743 54. Ma X-F, Gustafson JP. Genome evolution of allopolyploids: a process of cytological
744 and genetic diploidization. Cytogenet Genome Res. 2005;109: 236–249.
745 doi:10.1159/000082406
746 55. Balloux F, Lehmann L, de Meeûs T. The Population Genetics of Clonal and Partially
747 Clonal Diploids. Genetics. 2003;164: 1635–1644. doi:10.1093/genetics/164.4.1635
748 56. Carlton PM, Davis RE, Ahmed S. Nematode chromosomes. Genetics. 2022.
749 doi:10.1093/genetics/iyac014
750 57. Masterson J. Stomatal size in fossil plants: evidence for polyploidy in majority of
751 angiosperms. Science. 1994;264: 421–424. doi:10.1126/science.264.5157.421
752 58. Shen Y, Li W, Zeng Y, Li Z, Chen Y, Zhang J, et al. Chromosome-level and
753 haplotype-resolved genome provides insight into the tetraploid hybrid origin of
754 patchouli. Nat Commun. 2022;13: 1–15. doi:10.1038/s41467-022-31121-w
755 59. Dodsworth S, Chase MW, Leitch AR. Is post-polyploidization diploidization the key to
756 the evolutionary success of angiosperms? Bot J Linn Soc. 2016;180: 1–5.
757 doi:10.1111/boj.12357
758 60. Harris S, Rudnicki KS, Haber JE. Gene conversions and crossing over during
759 homologous and homeologous ectopic recombination in Saccharomyces cerevisiae.
760 Genetics. 1993;135: 5–16. doi:10.1093/genetics/135.1.5
761 61. Mansai SP, Innan H. The power of the methods for detecting interlocus gene
762 conversion. Genetics. 2010;184: 517–527. doi:10.1534/genetics.109.111161
763 62. Hollister JD. Polyploidy: adaptation to the genomic environment. New Phytol.
764 2015;205: 1034–1039. doi:10.1111/nph.12939

765 63. Paquin C, Adams J. Frequency of fixation of adaptive mutations is higher in evolving
766 diploid than haploid yeast populations. Nature. 1983;302: 495–500.
767 doi:10.1038/302495a0
768 64. Otto SP, Whitton J. Polyploid incidence and evolution. Annu Rev Genet. 2000;34:
769 401–437. doi:10.1146/annurev.genet.34.1.401
770 65. Zörgö E, Chwialkowska K, Gjuvsland AB, Garré E, Sunnerhagen P, Liti G, et al.
771 Ancient evolutionary trade-offs between yeast ploidy states. PLoS Genet. 2013;9:
772 e1003388. doi:10.1371/journal.pgen.1003388
773 66. Castagnone-Sereno P, Mulet K, Danchin EGJ, Koutsovoulos GD, Karaulic M, Da
774 Rocha M, et al. Gene copy number variations as signatures of adaptive evolution in
775 the parthenogenetic, plant-parasitic nematode Meloidogyne incognita. Mol Ecol.
776 2019;26: 906. doi:10.1111/mec.15095
777 67. Pogorelko GV, Juvale PS, Rutter WB, Hütten M, Maier TR, Hewezi T, et al. Re-
778 targeting of a plant defense protease by a cyst nematode effector. Plant J. 2019;98:
779 1000–1014. doi:10.1111/tpj.14295
780 68. Kihika R, Tchouassi DP, Ng'ang'a MM, Hall DR, Beck JJ, Torto B. Compounds
781 Associated with Infection by the Root-Knot Nematode, Meloidogyne javanica,
782 Influence the Ability of Infective Juveniles to Recognize Host Plants. J Agric Food
783 Chem. 2020;68: 9100–9109. doi:10.1021/acs.jafc.0c03386
784 69. Song H, Lin B, Huang Q, Sun T, Wang W, Liao J, et al. The Meloidogyne javanica
785 effector Mj2G02 interferes with jasmonic acid signalling to suppress cell death and
786 promote parasitism in Arabidopsis. Mol Plant Pathol. 2021;22: 1288–1301.
787 doi:10.1111/mpp.13111
788 70. Sellers GS, Jeffares DC, Lawson B, Prior T, Lunt DH. Identification of individual root-
789 knot nematodes using low coverage long-read sequencing. PLoS One. 2021;16:
790 e0253248. doi:10.1371/journal.pone.0253248

791 71. PacificBiosciences. IsoSeq3. Github; 2022. Available:
792 https://github.com/PacificBiosciences/IsoSeq
793 72. Winter M. asmapp: ASMAPP assembly appraisal workflow. Built in snakemake,
794 ASMAPP performs many basic and intermediate assembly appraisal tasks. Github;
795 2022. Available: https://github.com/mrmrwinter/asmapp
796 73. Guan D, McCarthy SA, Wood J, Howe K, Wang Y, Durbin R. Identifying and
797 removing haplotypic duplication in primary genome assemblies. Bioinformatics.
798 2020;36: 2896–2898. doi:10.1093/bioinformatics/btaa025
799 74. Luo J, Lyu M, Chen R, Zhang X, Luo H, Yan C. SLR: a scaffolding algorithm based
800 on long reads and contig classification. BMC Bioinformatics. 2019;20: 1–11.
801 doi:10.1186/s12859-019-3114-9
802 75. Durand NC, Robinson JT, Shamim MS, Machol I, Mesirov JP, Lander ES, et al.
803 Juicebox Provides a Visualization System for Hi-C Contact Maps with Unlimited
804 Zoom. Cell Syst. 2016;3: 99–101. doi:10.1016/j.cels.2015.07.012
805 76. Smit AFA, Hubley R, Green P. RepeatModeler Open-1.0. 2008--2015. Seattle, USA:
806 Institute for Systems Biology Available from: httpwww repeatmasker org, Last
807 Accessed May. 2015;1: 2018.
808 77. Smit AFA, Hubley R, Green P. RepeatMasker Open-4.0. 2013--2015. 2015.
809 78. Holt C, Yandell M. MAKER2: an annotation pipeline and genome-database
810 management tool for second-generation genome projects. BMC Bioinformatics.
811 2011;12: 491. doi:10.1186/1471-2105-12-491
812 79. Campbell MS, Holt C, Moore B, Yandell M. Genome Annotation and Curation Using
813 MAKER and MAKER-P. Curr Protoc Bioinformatics. 2014;48: 4.11.1–39.
814 doi:10.1002/0471250953.bi0411s48

80. Ondov BD, Treangen TJ, Melsted P, Mallonee AB, Bergman NH, Koren S, et al. Mash: fast genome and metagenome distance estimation using MinHash. Genome Biol. 2016;17: 132. doi:10.1186/s13059-016-0997-x

81. Simão FA, Waterhouse RM, Ioannidis P, Kriventseva EV, Zdobnov EM. BUSCO: assessing genome assembly and annotation completeness with single-copy orthologs. Bioinformatics. 2015;31: 3210–3212. doi:10.1093/bioinformatics/btv351

82. Marçais G, Kingsford C. A fast, lock-free approach for efficient parallel counting of occurrences of k-mers. Bioinformatics. 2011;27: 764–770. doi:10.1093/bioinformatics/btr011

83. Tang H, Bowers JE, Wang X, Ming R, Alam M, Paterson AH. Synteny and collinearity in plant genomes. Science. 2008;320: 486–488. doi:10.1126/science.1153917

84. Tang H, Krishnakumar V, Li J. jcvi: JCVI utility libraries. 2015. doi:10.5281/zenodo.31631

85. Altschul SF, Gish W, Miller W, Myers EW, Lipman DJ. Basic local alignment search tool. J Mol Biol. 1990;215: 403–410. doi:10.1016/S0022-2836(05)80360-2

86. Bernt M, Donath A, Jühling F, Externbrink F, Florentz C, Fritzsch G, et al. MITOS: improved de novo metazoan mitochondrial genome annotation. Mol Phylogenet Evol. 2013;69: 313–319. doi:10.1016/j.ympev.2012.08.023

87. Li H, Handsaker B, Wysoker A, Fennell T, Ruan J, Homer N, et al. The Sequence Alignment/Map format and SAMtools. Bioinformatics. 2009;25: 2078–2079. doi:10.1093/bioinformatics/btp352

88. Gurevich A, Saveliev V, Vyahhi N, Tesler G. QUAST: quality assessment tool for genome assemblies. Bioinformatics. 2013;29: 1072–1075. doi:10.1093/bioinformatics/btt086

841

842 # Supporting information

843 **S1 Fig: Length and quality statistics of concatenated and quality controlled PacBio**
844 **HiFi libraries.**

845 **S2 Fig: Length and quality statistics of concatenated and quality controlled Oxford**

846 **Nanopore libraries.**

847 **S3 Fig: Total cumulative length over number of scaffolds.**

848 **S4 Fig: Blobplot of contamination in our *Meloidogyne javanica* assembly**

849 **S5 Fig: BUSCO v5 results.**

850 **S6 Fig: Assembly-wide distributions of coverage**

851 **S7 Fig: Scaffold-level distributions of coverage**

852 **S8 Fig: Coverage depth of individual bases across scaffolds.**

853 **S9 Fig: Subgenome phased dendrogram of scaffolds.**

854 **S1 Table: Descriptive statistics of assembly and its contemporaries**

855 **S2 Table: Tabular breakdown of repeat annotation from *RepeatMasker*.**

856 **S3 Table: Full table of results from structural annotation with MAKER3.**

857 **S4 Table: List of pairs that share CDS and amount of shared links.**

858 **S5 Table: Validation of homoeologous pairings.**

859 **S6 Table: Summary of the longest 33 scaffolds.**